Author Manuscript

Author Manuscript

Author Manuscript

Author Manuscript

HHS Public Access

Author manuscript

Invest Ophthalmol Vis Sci. Author manuscript; available in PMC 2019 June 05.

Published in final edited form as:

Invest Ophthalmol Vis Sci. 2007 October ; 48(10): 4407–4420. doi:10.1167/iovs.07-0432.

SOD2 Knockdown Mouse Model of Early AMD

Verline Justilien[1], **Ji-Jing Pang**[2], **Kutralanathan Renganathan**[3], **Xianquan Zhan**[3], **John W. Crabb**[3], **So Ra Kim**[4], **Janet R. Sparrow**[4], **William W. Hauswirth**[2], and **Alfred S. Lewin**[1]

[1]Department of Molecular Genetics, University of Florida, Gainesville, Florida

[2]Department Ophthalmology University of Florida, Gainesville, Florida

[3]Cole Eye Institute and Lerner Research Institute, Cleveland Clinic, Cleveland, Ohio

[4]Department of Ophthalmology, Columbia University, New York, New York

Abstract

Purpose—To test the hypothesis that oxidative injury to the retinal pigment epithelium (RPE) may lead to retinal damage similar to that associated with the early stages of age-related macular degeneration (AMD).

Methods—A ribozyme that targets the protective enzyme manganese superoxide dismutase (MnSOD) was expressed in RPE-J cells, and adeno-associated virus (AAV) expressing the ribozyme gene was injected beneath the retinas of adult C57BL/6 mice. The RPE/choroid complex was examined for SOD2 protein levels and protein markers of oxidative damage using immunoblot analysis and LC MS/MS-identification of proteins and nitration sites. Lipids were extracted from retinal tissue and analyzed for the bis-retinoid compounds A2E and iso-A2E. The mice were analyzed by full-field electroretinography (ERG) for light response. Light and electron microscopy were used to measure cytological changes in the retinas.

Results—The treatment of RPE-J cells with Rz432 resulted in decreased MnSOD mRNA and protein as well as increased levels of superoxide anion and apoptotic cell death. When delivered by AAV, Rz432 reduced MnSOD protein and increased markers of oxidative damage, including nitrated and carboxyethylpyrrole-modified proteins in the RPE-choroid of mice. Ribozyme delivery caused a progressive loss of electroretinograph response, vacuolization, degeneration of the RPE, thickening of Bruch's membrane, and shortening and disorganization of the photoreceptor outer and inner segments. Progressive thinning of the photoreceptor outer nuclear layer resulted from apoptotic cell death. Similar to the eyes of patients with AMD, ribozyme-treated eyes exhibited increased autofluorescence and elevated levels of A2E and iso-A2E, major bis-retinoid pigments of lipofuscin.

Conclusions—These results support the hypothesis that oxidative damage to the RPE may play a role in some of the key features of AMD.

Corresponding author: Alfred S. Lewin, Box 100266, University of Florida College of Medicine, Gainesville, FL 32610-0266; lewin@ufl.edu.

Disclosure: **V. Justilien**, None; **J.-J. Pang**, None; **K. Renganathan**, None; **X. Zhan**, None; **J.W. Crabb**, None; **S.R. Kim**, None; **J.R. Sparrow**, None; **W.W. Hauswirth**, Applied Genetic Technologies Corporation (P); **A.S. Lewin**, None

Author Manuscript Author Manuscript Author Manuscript Author Manuscript

Age-related macular degeneration (AMD) accounts for the majority of irreversible severe vision loss in the elderly population of industrialized countries.[1–4] The progressive loss of vision that occurs in AMD is a result of injury to the macular photoreceptors, RPE, Bruch's membrane (an extracellular matrix between the RPE and the choriocapillaris consisting of collagenous and elastic layers), and the choroid.[5] This is a heterogeneous disease typically categorized as either "dry" or "wet" AMD. Dry AMD is associated with early-stage disease and subretinal deposits known as drusen that may cause little or no loss of vision. However, dry AMD may also lead to regional atrophy of the photoreceptors in the macula, with significant vision loss. Wet, or neovascular, AMD is late-stage disease and is always associated with substantial loss of central vision due to macular edema and scarring. The events that precipitate macular injury are not known. It is postulated, however, that several genetic and environmental risk factors act in concert to determine one's susceptibility to AMD.[6,7] Recently, strong genetic evidence has shown certain polymorphisms occurring in genes encoding complement factor H (CFH), factor B, complement component 2, and the LOC387715 locus, which encodes a heat shock serine protease as major risk factors for AMD.[8–16] The high risk for AMD associated with the 402H allele of complement factor H has added to increasing evidence from several sources that progression to the disease state is an inflammatory process. But there may be several initiating events that contribute to the formation of this disease. Risk factors for AMD such as old age, smoking, and blue-light illumination have increased oxidative stress as a common denominator. In contrast, a diet or a dietary supplement rich in antioxidants reduces the risk of progression to wet AMD in select individuals. The generation of toxic oxidants may damage the retina/RPE/choroid complex and may be a key component in the pathogenesis of AMD.[17] Although the accumulated impact of oxidative damage affect all older retinas, those individuals at genetic risk because they carry the wrong version of CFH, for example, have a greater risk of the development of AMD.

Reactive oxygen and nitrogen species (ROS/RNS) include such chemically active molecules as superoxide anion (O^{2-}), hydrogen peroxide (H_2O_2), the hydroxyl radical (OH^-), singlet oxygen ($^1O_2$), nitric oxide (NO*), and peroxynitrite anion ($ONOO^-$).[18] ROS/RNS participate in damaging reactions that can alter structures of macromolecules to yield peroxides, oxidized proteins, and DNA strand breaks that are precursors of cell death and disease. Under normal physiological conditions, mitochondria are the major intracellular source of ROS, producing superoxide anion as a normal byproduct of oxidative metabolism.[18] The antioxidant enzyme manganese superoxide dismutase (MnSOD) encoded by the nuclear gene *SOD2* is localized in the mitochondrial matrix and converts the superoxide anion produced by aerobic respiration to hydrogen peroxide, a critical step in the cell's defense against oxidative stress.

In an attempt to study the effects of oxidative damage to the RPE, we used AAV-ribozyme–mediated knockdown of the mRNA of SOD2 in the RPE of wild-type mice. Mice homozygous for a disruption of SOD2 do not live beyond 2.5 weeks after birth.[19] Sandbach et al.[20] characterized the pathologic features in the retinas of *SOD2*-deficient mice. In this model, however, the increased oxidative burden is not limited to the RPE, where the primary lesion of AMD is thought to lie.[5]The AAV ribozyme approach allows somatic knockdown of SOD2 expression in normal adult tissue, thus circumventing the problem of the lethality of

Author Manuscript Author Manuscript Author Manuscript Author Manuscript

the SOD2 knockout. This approach has been successfully used to model other diseases.[21–23] In this article, we report the use of ribozymes to induce oxidative damage in the RPE of wild-type mice, as an approach to a possible animal model of early dry AMD. Typical of the human disease, we detected morphologic changes in the RPE and Bruch's membrane, accumulation of oxidatively modified proteins,[24] and increased levels of autofluorescence and the bis-retinoid pigments found in RPE and drusen.[25] These are all hallmarks of AMD.

Materials and Methods

Ribozyme Cloning and rAAV Vectors

DNA oligonucleotides coding for the active and inactive mouse/rat SOD2 ribozymes were cloned in an AAV packaging plasmid. The inactive ribozyme contained a G-to-C mutation at a conserved position in the catalytic core. Expression of the ribozymes was driven by the hybrid cytomegalovirus (CMV) enhancer and chicken β-actin (CBA) promoter. Within the same AAV packaging plasmid was a CMV promoter-green fluorescent protein (GFP) cassette to enable the area of retina transduced to be observed. The active and inactive ribozyme-GFP as well as a GFP-only construct were packaged into AAV1 capsids, according to published techniques.[26]

SOD2 Ribozyme Delivery to RPE-J Cells

RPE-J cells (ATCC, Rockville, MD) were grown in Dulbecco's modified Eagle's medium (DMEM; Cellgro; Mediatech, Inc., Herndon, VA) supplemented with 4% fetal bovine serum, nonessential amino acids, and penicillin/streptomycin at 32.5°C in 5% CO_2. The cells were plated on 10-cm dishes and transfected with plasmids containing SOD2 ribozymes according to the manufacturer's protocol for the transfection agent (Lipofectamine 2000; Invitrogen Corp., Carlsbad, CA). Transfection efficiency was determined by using flow cytometry based on the fraction of cells expressing the GFP marker. At 1, 2, and 4 days after transfection, the RPE-J cells were harvested, and the cell pellets were divided in two. Half of the pellet was used with an RNA isolation kit (Sigma-Aldrich, St. Louis, MO). Reduction of SOD2 mRNA was determined by RT-PCR using β-actin as an internal control. SOD2 and β-actin PCR products were resolved on a 7% polyacrylamide gel stained with SYBR green, and the products were quantitated (Storm Phosphoimager; GE Healthcare, Piscataway, NJ). The other half of the pellet was used to extract protein to perform Western blot analysis. Nitrocellulose membranes were reacted with a rabbit polyclonal antibody to manganese SOD and then goat anti-rabbit IgG horseradish peroxidase–conjugated secondary antibodies to detect the bound antibodies by enhanced chemiluminescence (ECL). Anti-mouse β-actin antibody was used as an internal control for protein loading.

Detection of ROS and Apoptosis in RPE-J Cells

To detect intracellular superoxide generation, we used dihydroethidium (DHE; Invitrogen-Molecular Probes, Eugene, OR), which is specifically oxidized by superoxide. RPE-J cells were transfected with the SOD2 ribozymes or GFP control plasmid. The red fluorescent signal was quantitated by using a microplate spectrofluorometer. To determine levels of

Author Manuscript Author Manuscript Author Manuscript Author Manuscript

apoptosis, we measured nucleosome release using a cell death detection ELISA kit (Roche Applied Science, Indianapolis, IN) according to the methods provided by the manufacturer.

Experimental Animals and Injection of rAAV

All animal procedures were performed in accordance with the NIH Guide for Care and Use of Laboratory Animals, the University of Florida Institutional Animal Care and Use Committee, and the ARVO Statement for the Use Animals in Ophthalmic and Vision Research. Mice were maintained in 12-hour light–dark regimen. The right eyes of DBAJ/1 and C57BL/6J mice were injected subretinally with 1 μL of 2.5×10^{12} particles per milliliter of active ribozyme vector, and the left eyes were injected with a control AAV expressing either inactive ribozyme plus GFP or GFP only. The injections were performed as described by Timmers et al.[27]

Detection of GFP Expression In Vivo

At 6 weeks after injection, mice from each group were killed. Their eyes were enucleated and briefly rinsed in PBS. The eyes were fixed overnight in 4% paraformaldehyde, incubated in increasing concentrations of sucrose, embedded in OCT medium, and frozen by dipping into isopentane-cooled liquid nitrogen. Frozen serial sections (12 μm) were cut with a cryostat and observed with a fluorescence microscope for GFP expression as a marker for AAV transduction.

MnSOD Protein Levels In Vivo

Levels of MnSOD protein were determined by Western blot analysis. Briefly, at 6 weeks after injection, mice treated with AAV-Rz432 or AAV-GFP were euthanatized. Their eyes were enucleated and rinsed briefly in PBS, and the anterior chamber and excess tissue were discarded. The neural retina was separated from the posterior eye cup containing the RPE/choroid under a dissecting microscope. Protein was extracted from the posterior eye cup in Laemmli sample buffer by sonication. Soluble lysate protein (20 μg) was separated on a 12% SDS polyacrylamide gel and electrotransferred to a nitrocellulose membrane. The membranes were then immunostained separately overnight with a rabbit polyclonal anti-SOD2 antibody (Stressgen, Victoria, BC, Canada) or a mouse monoclonal β-actin antibody that served as a loading control.

Detection of Markers of Oxidative Damage

At 4 months after injection, sections of retinas from mice treated with AAV Rz432 or AAV GFP were analyzed by immunohistochemistry for HNE-adducts (4-hydroxynonenal; Alpha Diagnostics International, Inc., San Antonio, TX), which is a marker of oxidative damage. Sections were incubated overnight at 4°C with primary antibodies followed by incubation with CY3 fluorescently labeled secondary antibodies for 1 hour at room temperature. Images were obtained with a fluorescence microscope.

Western blot analysis was used to analyze ocular tissues for nitrotyrosine and CEP (carboxyethylpyrrole) adducts. Immediately after death, the animals' eyes were excised, and the retina and posterior eye cup were isolated as described earlier. The tissues were rinsed with PBS containing 2 mM diethylenetriaminepentaacetic acid and 100 μM butylated

Author Manuscript Author Manuscript Author Manuscript Author Manuscript

hydroxytoluene (BHT), each tube was flushed with argon and sealed, and the tissues were flash frozen in liquid nitrogen and stored at −80°C until analysis. Before Western blot analysis, lipids were extracted with chloroform methanol[28] and protein extracted in 60 mM Tris-HCl (pH 6.8), containing 2% SDS, 10 mM dithiothreitol (DTT), 100 μM BHT, and 2 mM EDTA with repeated steps of homogenization and centrifugation (three times). Protein concentrations were approximated using the Bradford Assay and SDS polyacrylamide gel electrophoresis (SDS-PAGE) was performed according to Laemmli on 10% gels. To ensure equal sample loading, preliminary SDS-PAGE (Supplementary Fig. S1, available online at http://www.iovs.org/cgi/content/full/48/10/4407/DC1) was performed with approximately equal sample amounts, gels stained with Coomassie blue (Gel Code Blue; Pierce Biotechnology, Rockford, IL) and scanned (GS-710 densitometer and Quantity One software; Bio-Rad, Hercules, CA), and sample volumes were adjusted based on optical density to obtain equal staining for all samples in subsequent SDS-PAGE. Western blot analysis was performed as described elsewhere with electroblotting to polyvinylidene difluoride (PVDF) membrane.[29] Blots were incubated overnight at 4°C with 1 μg/mL primary antibody (mouse anti-nitrotyrosine monoclonal antibody; Upstate Biotechnology, Lake Placid, NY), or mouse anti-carboxyethylpyrrole monoclonal antibody. Secondary antimouse antibody was used at a 1:10,000 dilution; detection was by chemiluminescence using enhanced chemiluminescence (ECL). Immunoreactivity in the developed blots was quantified by densitometry as earlier.

Immunoprecipitation of Nitrotyrosine-Containing Proteins

Rabbit anti-nitrotyrosine polyclonal antibody (200 μg; Chemicon International, Temecula, CA) was incubated with immunopure immobilized protein G beads (400 μL; gently shaking, 2 hours), then washed with binding/washing buffer (0.14 M NaCl, 0.008 M sodium phosphate, 0.002 M potassium phosphate, and 0.01 M KCl at pH 7.4) to remove unbound antibody. The bound antibody was covalently cross-linked to immobilized protein G with disuccinimidyl suberate (DSS; final concentration 0.0025%) by gently shaking for 1 hour and then washed with elution buffer (pH 2.8) that contained a primary amine to remove any non–cross-linked antibodies. The cross-linked antibody-protein G beads were washed twice with binding/washing buffer. The protein preparation (120 μL; 136.4 μg) from mouse posterior eye cups was diluted with protein G binding/washing buffer (Pierce Biotechnology) and incubated with the immobilized antibody (gently rocking, 4°C, overnight). The protein G-antibody protein beads were then washed three times with the binding/washing buffer. The bound nitrated proteins were eluted with 62.5 mM Tris-HCl/2% SDS at pH 7.0 (60 μL, 60°C, 20 minutes, three times). The eluate (180 μL) that contained nitrated proteins was concentrated to 50 μL and was fractionated on a 12% SDS polyacrylamide gel (120 mA, 1.5 hours) that was then stained with Coomassie blue (GelCode Blue; Pierce Biotechnology), and bands were excised from the top to the bottom of the lane for LC MS/MS identification of proteins and nitration sites.

Mass Spectrometric Identification of Nitrated Protein

The gel-fractionated immunoprecipitation products were subjected to digestion in situ with trypsin and online LC-MS/MS analysis (QTOF2 mass spectrometer; Waters Corp., Milford, MA). The tryptic peptides were separated on a 75-μm × 5-cm C18 column (5 m particle size,

Author Manuscript Author Manuscript Author Manuscript Author Manuscript

300 Å pore size; Vydac, with a CapLC system; Waters), with aqueous formic acid/acetonitrile solvents and a flow rate of ~250 nL/min and sprayed directly into the mass spectrometer. Protein identification was performed with the spectrometer system software (Masslynx, ver, 4.1; Waters), a search engine (Mascot ver. 2.1; Matrix Science, Boston, MA), and the Swiss-Protein sequence database (Swiss Prot, http://www.expasy.org; provided in the public domain by the Swiss Institute of Bioinformatics, Geneva, Switzerland). The protein modifications selected in the database search were tyrosine nitration (Y), deamidation (N, Q), oxidation (M), and carbamidomethylation (C). Tyrosine-nitration sites were verified by manual examination of MS/MS spectra. Each nitrated peptide was examined by BLAST analysis against the Swiss-Protein and National Center for Biotechnology (NCBI) databases.

Electroretinography

Animals were dark adapted overnight before electroretinographic (ERG) analysis, and all procedures were performed under dim red light. Full-field ERGs were obtained in a Ganzfeld illumination dome. The a-and b-wave responses were obtained in the dark-adapted state by flashing increasing intensities of light (0.02, 0.18, and 2.68 cd-s/m^2), and electrical responses were recorded simultaneously from both eyes (UTAS-ER 2000 Visual Electrodiagnostic System; LKC Systems Inc., Gaithersburg, MD). Intervals between flashes (15–60 seconds) were increased with increasing flash intensities. Five recordings were taken and averaged per flash intensity.

Light and Electron Microscopy

For light microscopy, at 1, 2, and 4 months after treatment, groups of three mice treated with AAV-Rz432 or AAV-GFP were killed. The eyes were then fixed and cryosectioned as described earlier. The sections were stained with hematoxylin and eosin. The outer nuclear layer thickness was quantitated (Axiovision 4.4 software; Carl Zeiss Meditec, Inc., Dublin, CA). For electron microscopy, at 4.5 months after treatment, 5 mice from each treatment group were given an overdose of sodium pentobarbital and then immediately perfused with 4% paraformaldehyde and 2% glutaraldehyde in 0.1 M PBS buffer (pH 7.4). The eyes were enucleated and immersed in 4% paraformaldehyde and 2% glutaraldehyde for further fixation overnight. Eyes were postfixed with 1% osmium tetroxide, 0.1 M sodium cacodylate-HCl buffer (pH 7.4), and dehydrated through a series of increasing ethanol concentrations leading up to propylene oxide. Eyes were embedded in epoxy resin and sections of 80 to 100 nm were cut and examined by transmission electron microscope. The thickness of Bruch’s membrane was measured on 20,00× micrographs taken of five individual active or inactive Rz432-treated retinas. Three measurements of Bruch’s membrane were made for each retina.

Retinal Apoptotic Cell Death

TUNEL staining was performed on frozen sections obtained as described for light microscopy. Lysates obtained from the posterior eye cups of mice 6 weeks after injection with AAV-Rz432 or AAV-GFP were used to quantitate levels of apoptotic cell death with a kit for an ELISA-based nucleosome release assay (Cell Death Detection ELISA kit; Roche Applied Science).

Author Manuscript Author Manuscript Author Manuscript Author Manuscript

Autofluorescence Analysis

At 4 months after injection, eyes were enucleated, briefly rinsed in PBS, and fixed for 1 hour in 4% paraformaldehyde, and the cornea and lens were then removed. The entire retina was carefully dissected from the posterior RPE/choroid/sclera eye cup. Flatmounts were mounted in antifade medium with 4′,6′-diamino-2-phenylindole (DAPI; Vectashield; Vector Laboratories, Burlingame, CA) and examined for fluorescence (TCS SP2 AOBS Spectral Confocal Microscope with Confocal Software Version 2.61, Build 1537; Leica, Deerfield, IL).

Measurement of Bis-retinoid Compounds

A2E and iso-A2E levels in the posterior eye cups of four AAV-Rz432–treated or control eyes were quantified by HPLC as described by Kim et al.[30] Briefly, the cornea and lens were removed by cutting circumferentially around the limbus. The posterior eye cups containing the sclera, choroid, RPE, neural retina, and vitreous, were solubilized in 0.1% Triton X-100 and extracted three times with chloroform-methanol (2:1). The extract was analyzed by reversed-phase HPLC on a C18 column (4 × 150 mm) and an acetonitrile and water gradient with 0.1% trifluoroacetic acid (gradient; 90%–100%, 0–10 minutes; 100% acetonitrile, 10–20 minutes; flow rate, 0.8 mL/min; and monitoring at 430 nm). Integrated peak areas were determined by computer (Empower software; Waters Corp.), and picomolar concentrations were calculated by using external standards of A2E.

Results

Ribozyme Knockdown of MnSOD in RPE Cells

As a precursor to testing SOD2 Rz432 (Fig. 1A) in mice, its effectiveness was tested in a rat retinal pigment epithelial cell line (RPE-J). RPE-J cells were transfected with a plasmid containing Rz432 driven by the hybrid CMV enhancer-chicken β-actin promoter and a GFP marker gene, to allow us to monitor cells expressing Rz432 (Fig. 1B). Cells were also transfected with a plasmid expressing only GFP to serve as a control. We typically achieved transfection efficiencies of 60% to 70% as measured by flow cytometry. Total RNA and protein were harvested from the RPE-J cells at 1, 2, and 4 days after transfection. Levels of SOD2 mRNA and protein were analyzed with RT-PCR and Western blot analysis, respectively, using β-actin as an internal control. Two days after transfection, RPE-J cells treated with Rz432 showed an approximate 32% (Fig. 2A) and 60% (Fig. 2B) reduction of SOD2 mRNA and protein levels, respectively, compared with control transfected cells. Because our transfection efficiency was only slightly better than 60%, the ribozyme must have been effective in reducing MnSOD synthesis in transduced cells. The return of SOD2 mRNA and protein toward control levels at 4 days after treatment was probably due to dilution of the ribozyme plasmid after transient transfection and continued cell division.

Suppression of SOD2 and Apoptosis in RPE Cells

The suppression of MnSOD expression is expected to cause an increase in levels of superoxide anion. Our maximum knockdown of MnSOD was achieved at two days after treatment of the RPE-J cells with Rz432. We therefore selected that time point to document

Author Manuscript Author Manuscript Author Manuscript Author Manuscript

superoxide anion levels by using the dye DHE. RPE-J cells treated with Rz432 showed increased red signal of oxidized DHE generated by increased superoxide anion levels compared with the control cells treated with GFP. Quantitation of the red fluorescent signal revealed a greater than 33% increase in the levels of reactive oxidants ($P < 0.03$) which can induce apoptosis.[31] One of the hallmark features of apoptosis is fragmentation of DNA and the release of nucleosomes into the cytoplasm.[32] To investigate whether apoptosismediated cell death occurred after ribozyme treatment, an ELISA-based nucleosome-release assay was performed. At 2 days after transfection, RPE-J cells treated with Rz432 showed a modest (13%) but statistically significant increase in nucleosome release ($P < 0.05$).

Effect of Ribozyme Expression MnSOD in the RPE

Because loss of function of the RPE is thought to initiate AMD,[5] Rz432 was targeted to the RPE to explore whether biochemical and morphologic changes in the retina could be induced that replicate the human disease. Auricchio et al.[33] have shown that serotype 1 (AAV1) predominantly transduces the RPE when delivered subretinally. For in vivo experiments, to achieve robust expression of Rz432 that is predominantly in the RPE, we used the potent chimeric CBA promoter and packaged our construct in AAV1 capsids. The construct also contained a GFP marker gene to visualize the area of the retina transduced by our vector. The AAV1-Rz432-GFP vector was injected in the subretinal space of adult wild-type C57Bl/6 mice. To confirm expression of Rz432-GFP in the RPE, paraformaldehyde-fixed cryostat sections were analyzed for GFP expression. We observed Rz432-GFP expression predominantly in the RPE layer, with scattered expression in the photoreceptor cells (Fig. 3A). We note that *all* of the eyes analyzed in our study were injected with a virus expressing GFP from the CMV or CBA promoter: Control eyes lacked the ribozyme or contained an inactive ribozyme.

To determine whether Rz432 causes knockdown of MnSOD protein in vivo, we performed immunoblot analysis for MnSOD with total protein from RPE/choroid tissues of AAV-Rz432- and AAV-GFP-treated control eyes. β-Actin was used as a loading control. At 6 weeks after injection we observed a significant decrease of MnSOD protein in Rz432-treated versus controltreated retinas (Fig. 3B). Because AAV1 transduced RPE cells almost exclusively, greater MnSOD knockdown may have been masked by cells of the choroid or adherent photoreceptor cells that did not express ribozyme and were still expressing MnSOD.

Effect of SOD2 Suppression on Oxidative Injury in the RPE

Prolonged, increased levels of ROS can overwhelm antioxidant defenses leading to oxidative modification of proteins, lipids, and DNA. Nitrotyrosine, 4-hydroxy-2-nonenal (4-HNE), and carboxyethylpyrrole (CEP) are some of the markers that have been used to assess long-term oxidative damage.[24,34] Elevated concentrations of superoxide anion in the presence of nitric oxide can form peroxynitrite which is able to generate nitrotyrosine residues in proteins and lead to impaired protein function.[35] Levels of nitrotyrosine residues in proteins of AAV Rz432 versus AAV GFP-treated RPE/choroid were examined by Western blot analysis. We found increased immunostaining for nitrotyrosine across a large range of molecular weights in Rz432-treated versus GFP control RPE/choroid (Fig. 4A). CEP protein

Author Manuscript Author Manuscript Author Manuscript Author Manuscript

adducts, generated from the oxidation of docosahexaenoate (DHA)-containing lipids, are more abundant in Bruch's membrane[24]and plasma[29] from AMD than normal donors, and stimulate neovascularization in vivo.[36] Immunoblot analysis was also used to assess levels of CEP after Rz432 treatment and showed a moderately significant increase of staining for protein bands immunoreactive with CEP (Fig. 4B). Quantitation of the optical intensities of the immunoreactive bands showed an approximately 2- to 2.5-fold increase in mean nitrotyrosine and CEP in Rz432-treated eyes relative to control eyes. As has been noted by others,[37] oxidative modification of proteins is not uniform, and some proteins are more susceptible than others. It may be easier to detect modification of highly abundant proteins using these methods. As seen in Figures 4A and 4B, some protein oxidation occurs in normal animals, but the level is elevated with increased oxidative stress.

The aldehyde 4-HNE is a specific and stable end product of lipid peroxidation that is generated as a consequence of oxidative stress.[38] Retinal sections from mice treated with AAV-Rz432 and AAV-GFP were incubated with an antibody that recognizes 4-HNE Michael adducts with cysteine, histidine, and lysine residues.[39] Rz432-treated retinas also exhibited increased staining for 4-HNE reaction products in the RPE and photoreceptor outer/inner segments (Supplementary Fig. S2, http://www.iovs.org/cgi/content/full/48/10/4407/DC1). Increased levels of markers of oxidative damage result from chronic exposure to oxidants. Therefore, our results indicate that, as a result of ribozyme-mediated decrease of MnSOD, we were able to establish a chronic environment of oxidative stress in the RPE.

MS Identification of Nitrated Proteins

An anti-nitrotyrosine antibody was used to immunoprecipitate nitrated proteins from Rz432-treated posterior eye cup extracts. Immunoprecipitates were separated by SDS-PAGE, the gel slices were subjected to in situ tryptic digestion, and the resultant peptides were analyzed by LC MS/MS. Tyrosine nitration sites were detected in 8 different peptides (Table 1; Supplementary Figs. S3–S10, http://www.iovs.org/cgi/content/full/48/10/4407/DC1). Each nitrated peptide was detected as a "single hit" peptide, and the identity of the parent protein was evaluated based on expectation [E]-values obtained from Blast searches with the determined peptide sequences. These results indicate that nitrated transducin-like enhancer protein 3 and nitrated elastase 1 were unequivocally identified, and nitrated FGF receptor 2 and nitrated early development regulatory protein 2 were highly likely to be identified. Database search results with the other four nitrated peptides provided tentative protein identifications. The results are summarized in Table 1.

Loss of Electrophysiological Responses

AMD may be associated with geographic atrophy, the degeneration of photoreceptors in the macular region of the retina, associated with atrophied or malfunctioning RPE. While not routinely used as a tool for the diagnosis of AMD, electroretinography can be used to detect loss of photoreceptor function arising from retinal diseases, including AMD. To assay the effect of SOD2 knockdown on the ability of the retinas of mice to respond to light, adult C57Bl/6 mice were injected subretinally with AAV expressing active Rz432. Other groups of mice were injected with AAV expressing GFP to serve as control subjects. At 1, 2, 4, and 6 months after injection, we performed full-field scotopic (dark adapted) electroretinography

Author Manuscript Author Manuscript Author Manuscript Author Manuscript

(ERG) to measure the response of treated eyes to light. Though the variation in ERG amplitudes between animals can be considerable, the a- and b-wave amplitudes in both eyes of a single untreated mouse is the same. Therefore, we analyzed the results as the ratio of a- and b-wave amplitudes for the AAVRz432- and AAV-GFP-treated eyes of each mouse. Figure 5 presents the average of these ratios of Rz-treated to control amplitudes over a 6-month period. We observed a progressive loss of a- and b-wave responses between 2 and 4 months after injection. No significant changes were observed in a- or b-wave response at the 1- or 2-month time points. However, by 4 months after injection, Rz432-treated eyes showed significant loss of ERG response with an average of 33% and 41% decrease in a- and b-waves, respectively, compared with control-treated eyes. The a-wave response continued to decline from the 4- to 6-month time point, whereas the b-wave response appeared to plateau. To show that the effect we observed was not specific for C57BL/6 mice, we also treated DBAJ/1 mice with active or inactive Rz432. DBAJ/1 mice showed a similar progressive loss of a- and b-wave ERG amplitudes between 1 and 4 months after injection (data not shown). These results indicate that long-term suppression of MnSOD in the RPE was necessary to elicit functional changes in the retina.

Effect of MnSOD Suppression on the Structure of the Outer Retina

In addition to functional decay, treated retinas also exhibited morphologic damage at increasing intervals after injection. By 1 month after injection with AAV-Rz432, the retinas began to exhibit loss of pigmentation in the RPE, though the neural retina appeared normal at this stage. From 2 to 4 months, we observed more pronounced changes to the RPE, such as vacuole formation and atrophy. By 2 months after injection, the outer (OS) and inner segments (IS) of the photoreceptors were shortened and disorganized, and the outer nuclear layer (ONL) was detectably thinner, indicating loss of photoreceptor cells (Fig. 6A). The progressive thinning of the ONL in Rz432-treated retinas was quantitated by measuring the thickness of the ONL at various time points. Measurements were taken at 400-μm increments from the optic nerve to the peripheral retina on both the inferior and superior portions of the retina. By 4 months after treatment, there was a 30% to 50% reduction in ONL thickness across retinas treated with Rz432 versus GFP control (Fig. 6B). This reduction was statistically significant ($P < 0.05$–$P < 0.01$) in the inferior hemisphere.

Dunaief et al.[40] have shown that in AMD, the RPE, and photoreceptors die by apoptosis. To determine whether the thinning of the ONL that we observed histologically was a result of apoptotic cell death of the photoreceptors, we performed TUNEL staining of retinas at 6 weeks after injection. Retinas treated with AAV-Rz432 showed increased TUNEL-positive staining specifically in the ONL (Fig. 6C). In eyes treated with AAV-Rz432, we counted 6.5 ± 1 TUNEL-positive nuclei per 100 nuclei in the ONL, whereas eyes treated with the control virus (AAV-GFP) showed less than one positive nucleus per 100. Because TUNEL-positive cells can arise from processes other than apoptosis, we used an ELISA-based nucleosome release assay to quantitate apoptosis. For this experiment, the anterior chamber, lens, and vitreous were removed and only the posterior chamber was used in the analysis. We observed a nearly twofold increase in nucleosome release in the ribozyme-treated retinas ($P < 0.003$; Fig. 6D). Apoptosis in mouse models of retinitis pigmentosa may be independent

Author Manuscript Author Manuscript Author Manuscript Author Manuscript

of caspase activation,[41,42] and we did not observe an increase in caspase 3 activation in the ribozyme-treated retinas in our model (data not shown).

Ultrastructural Evidence of Damage to the RPE and Bruch's Membrane

Electron microscopic analysis of retinas injected with the active or inactive Rz432 was performed after the 4-month time point. Several changes were observed in the RPE of retinas treated with active ribozyme, including deterioration of the basal lamina, formation of large vacuoles, and presence of irregular shaped nuclei (Fig. 7A). The vacuoles of the RPE were filled with membranous debris (Fig. 7B). The photoreceptor outer and inner segments were significantly shortened and disorganized (Fig. 7A). We also observed significant thickening of Bruch's membrane in the inner and outer collagenous zones as well as the middle elastin layer. Some of the eyes showed debris deposition between the plasma and basement membrane as well as between the basal laminar infoldings of the RPE which resembled basal laminar deposits observed in AMD eyes[43] (Fig. 7B). Morphometric measurements revealed that Bruch's membrane was an average of 40% thicker in eyes treated with AAV-Rz432 (1.37 ± 0.11 μm) compared with eyes treated with control virus expressing an inactive ribozyme plus GFP (0.8 ± 0.06 μm; $P < 0.005$).

Autofluorescent Aggregation after Rz432 Treatment

Fluorescence microscopy at 4.5 months after injection was used to determine whether the debris evident in electron micrographs of AAV-Rz432-treated eyes exhibited autofluorescent properties similar to lipofuscin. RPE cells of AAV-Rz432 eyes showed increased autofluorescent aggregates represented by the red fluorescence (Fig. 8). The aggregates varied in size, with some RPE cells presenting markedly larger granules.

To determine whether the fluorescent aggregates in the RPE were lipofuscin-like, HPLC measurements were performed for A2E and iso-A2E, which are major bis-retinoid fluorescent chromophores in lipofuscin. The chromatographic peaks corresponding to A2E and iso-A2E were elevated in AAV-Rz432-treated eyes. Quantitation of the amount of A2E and iso-A2E in DBAJ/1 mice showed a greater than twofold increase of these lipofuscin chromophores in AAV-Rz432-treated eyes (Fig. 8B). The average concentration of A2E and iso-A2E combined was 9.03 picomoles per retina in treated eyes and 4.70 picomoles per retina in control eyes. C57BL/6 mice also showed an increase in A2E and iso-A2E levels that was less significant than in the DBAJ/1 mice. Our results are consistent with the findings of Kim et al.[30] who showed that A2E and iso-A2E accumulate at a slower rate in mice carrying the Met450 variant in Rpe65 (C57BL/6).

Discussions

AMD is a complex disease with both genetic and environmental risk factors. Therefore, it is unlikely that a single biochemical process is responsible for the occurrence of AMD. In this study, we used mice to investigate the hypothesis that excessive oxidative burden on the RPE may contribute to the development of AMD. While mice have no macula, we reasoned that manipulation of their oxidative defense mechanisms might reveal damage to Bruch's membrane and to the RPE that may contribute to the later manifestations of AMD, such as

Author Manuscript Author Manuscript Author Manuscript Author Manuscript

drusen accumulation, geographic atrophy, and choroidal neovascularization (CNV). Specifically, reactive oxygen species-mediated damage of RPE enzymes and membrane components may impair the transport functions of this monolayer. Damage to DNA, proteins, and lipids may also lead to apoptosis. Without proper support from the RPE, the photoreceptors may starve and accumulate waste products, leading to their apoptotic death.

We induced oxidative stress by selectively knocking down the expression of the antioxidant enzyme MnSOD. We selected MnSOD because of its vital role in cellular defense against ROS, thereby maximizing our chances of inducing oxidative stress–mediated cell dysfunction. In addition, a genetic polymorphism in the *SOD2* gene has been associated with wet AMD.[44] RPE cells from *SOD2* heterozygous mice, which have approximately 60% the level of MnSOD of wild-type mice, are significantly more susceptible to oxidative stress–mediated apoptotic cell death than are wild-type RPE cells.[45] Although $SOD2^{-/-}$ mice die soon after birth, Sandbach et al.[20] showed significant histopathological changes in the RPE and photoreceptors, even at 3 weeks after birth. These findings indicate that mice deficient in SOD2 display outer retinal changes in a shorter time than in other antioxidant enzyme knockouts such as GPX-1 and SOD1, which do not exhibit retinal damage until after 1 year of age.[46,47] Since the $SOD2^{-/-}$ mice die before reaching full maturity, additional changes to the outer retina may not have had time to develop.

There are numerous observations that support a possible role for oxidative tissue injury in the pathogenesis of AMD. Mice deficient in copper-zinc SOD (encoded by *SOD1*) develop drusen-like deposits that increase after prolonged exposure to light.[47] In humans, taking dietary supplements containing antioxidants and zinc slows the progression of early AMD to wet AMD.[48] Smoking, which has been reported to deplete antioxidant levels, correlates positively to developing later stages of AMD.[49–52] Espinosa-Heidmann et al.[53] showed that exposure of mice to cigarette smoke resulted in AMD-like features such as the formation of sub-RPE deposits, thickening of Bruch's membrane, and accumulation of deposits within Bruch's membrane. Finally, Crabb et al.[24] have shown that AMD Bruch's membrane/RPE/choroid tissues contain increased oxidatively modified proteins compared with age-matched control tissues. Our ribozyme-mediated depletion of MnSOD indicates that the RPE is particularly susceptible to oxidative stress and that increased oxidative burden to the RPE may lead to some of the pathologic features of dry AMD. In particular, we observed atrophy and pigmentary changes of the RPE, significant increase in the thickness of Bruch's membrane, progressive loss of retinal electrophysiological function,[54,55] increased burden of oxidatively modified proteins, and accumulation of the lipofuscin components A2E and iso-A2E. We also observed apoptotic death of photoreceptors in a pattern that reflected AAV-mediated transduction of the RPE. In this respect, our model differs from the human disease in which geographic atrophy is restricted to the central retina.

The accumulation of protein markers of oxidative stress that we observed as a result of SOD2-knockdown (Fig. 4, Table 1) are also reminiscent of damage to the macular proteome in donor eyes of patients with AMD.[24] In particular, docosahexaenoate lipid-derived oxidative modifications (CEP-protein adducts) are more abundant in AMD than in normal Bruch's membrane. In addition, we observed an increase in nitrated proteins in ribozyme-treated RPE, although the functional significance of the proteins identified as nitrated

Author Manuscript Author Manuscript Author Manuscript Author Manuscript

remains unknown. These results provide the groundwork for further studies to determine whether the impaired function of any of these proteins contributes to disease in the RPE. Nitration has not been examined yet in the eyes of patients with AMD, but the present results coupled with observations of elevated nitrotyrosine immunoreactivity in AMD plasma (Gu et al., manuscript submitted) suggest that nitrotyrosine may be a marker for AMD-related damage that should be examined further in patients.

An increase in lipofuscin-mediated autofluorescence, such as we observed in AAV-Rz-treated eyes, is thought to be a characteristic of recently diagnosed AMD.[56] Build-up of lipofuscin generally precedes photoreceptor degeneration. Unusual vacuoles begin appearing in the RPE of ribozyme-treated eyes by 2 months after injection. The implication is that although phagocytosis of photoreceptor outer segments continues in the treated eyes, metabolic processing of ingested membranes is defective. The increase in the bis-retinoids A2E and iso-A2E that we observed in our mouse model should accentuate oxidative damage to the RPE, since A2E can act as a photosensitizer, generating singlet oxygen on blue light irradiation.[57] Irradiation of RPE cells laden with lipofuscin initiates a caspase cascade, resulting in apoptotic cell death.[58] The presence of autofluorescent aggregates in oxidatively stressed retinas (Fig. 8A), leads us to wonder whether protein markers of drusen (complement components, annexins, apolipoprotein E) might accumulate in these retinas. Such a proteomic analysis is beyond the scope of this initial study, especially since drusen were not observed.

In most of the current models used to study RPE oxidative stress, acute and high doses of either chemical treatments or light exposure are used.[59–61] In addition, in some studies, RPE cell lines are used that may not accurately reflect the behavior of this monolayer in vivo. Our system models the in vivo conditions in that we established a chronic increase in oxidative stress that led to progressive functional and histologic changes to the retina. It was of no surprise that we did not observe any changes at 1 month after injection: First, gene expression mediated by AAV1 transduction takes 2 weeks after injection to reach peak levels.[33] Second, the impact of oxidative stress may be cumulative. Cellular defense mechanisms may become overloaded resulting in histologic and functional changes that we observed in the retina beginning at approximately 2 months after injection.

The retinal damage we observed after RPE-specific ribozyme expression is consistent with the hypothesis that the primary lesion in AMD lies in the RPE.[5] In our model, we observed histologic changes in the RPE that preceded structural changes in the photoreceptor layers and the loss of the retinal function. In addition, we have determined that expressing Rz432 specifically in the photoreceptors (by using an opsin promoter to drive expression of the ribozyme) caused only a small loss of ERG and minor histologic changes that were limited to the photoreceptors (data not shown). We did not observe any changes in the RPE. Taken together, these observations indicate that the apoptosis we saw in the photoreceptors and the loss of ERG response was due to oxidative damage in the RPE.

We found a more significant thinning of the inferior portion of the retina of mice injected with AAV-Rz432. The inferior portion of the retina is exposed to more light than the superior hemisphere. Therefore, the more severe changes that we observed in the inferior

Author Manuscript Author Manuscript Author Manuscript Author Manuscript

hemisphere may be due to increased susceptibility to photooxidative stress, and light-mediated retinal damage resulting from a lack of MnSOD. Our observations are consistent with the findings of others that exposure of the retina to light may accelerate the progression and severity of AMD and certain forms of retinitis pigmentosa.[62–64] Imamura et al.[47] showed that a lack of cytoplasmic SOD in conjunction with increased light exposure causes increased drusen formation in mice.

It is likely that a longer period after treatment with AAVRz432 is necessary for the development of significant drusen and CNV, suggesting that additional factors, in conjunction with increased oxidative burden, may be needed for progression of the disease. We may combine treatment of SOD2 ribozymes with overexpression of VEGF, which has been shown to induce CNV.[65] Another approach is to reduce SOD2 levels in other mouse models predisposed to developing AMD-like features, such as Ccr2/Ccl2 mice[66] and aged mice exhibiting the apolipoprotein E4 genotype.[67] These mice do not begin to show indications of AMD until approximately 1 year of age. By promoting oxidative stress, these changes may be induced to occur earlier. Mice such as the *Ccr2*$^{-/-}$, *Ccl2*$^{-/-}$, and *SOD1*$^{-/-}$ that naturally exhibit CNV, do so late in life. Consequently, our SOD2 ribozymes may induce CNV if used in older mice.

Supplementary Material

Refer to Web version on PubMed Central for supplementary material.

Acknowledgments

Supported in part by National Eye Institute Grants EY016073 (ASL), EY14239, EY15638 (JWC) and EY12951 (JRS); EY13729, EY11123, EY08571, NS36302 (WWH); Ohio Grant BRTT 05-29; Macular Vision Research Foundation; Juvenile Diabetes Research Foundation; The Foundation Fighting Blindness; and The Steinbach fund. JWC is a Research to Prevent Blindness Senior Scientific Investigator.

References

1. Klein R, Klein BE, Jensen SC, Meuer SM. The five-year incidence and progression of age-related maculopathy: the Beaver Dam Eye Study. Ophthalmology. 1997;104:7–21. [PubMed: 9022098]
2. Leibowitz HM, Krueger DE, Maunder LR, et al. The Framingham Eye Study monograph: an ophthalmological and epidemiological study of cataract, glaucoma, diabetic retinopathy, macular degeneration, and visual acuity in a general population of 2631 adults, 1973–1975. Surv Ophthalmol. 1980;24:335–610. [PubMed: 7444756]
3. Mitchell P, Smith W, Attebo K, Wang JJ. Prevalence of age-relatedmaculopathy in Australia: the Blue Mountains Eye Study. Ophthalmology. 1995;102:1450–1460. [PubMed: 9097791]
4. Vingerling JR, Dielemans I, Hofman A, et al. The prevalence ofage-related maculopathy in the Rotterdam Study. Ophthalmology. 1995;102:205–210. [PubMed: 7862408]
5. Young RW. Pathophysiology of age-related macular degeneration. Surv Ophthalmol. 1987;31:291–306. [PubMed: 3299827]
6. Evans JR. Risk factors for age-related macular degeneration. Prog Retin Eye Res. 2001;20:227–253. [PubMed: 11173253]
7. Smith W, Assink J, Klein R, et al. Risk factors for age-relatedmacular degeneration: pooled findings from three continents. Ophthalmology. 2001;108:697–704. [PubMed: 11297486]
8. Dewan A, Liu M, Hartman S, et al. HTRA1 promoter polymorphism in wet age-related macular degeneration. Science. 2006;314:989–992. [PubMed: 17053108]

Author Manuscript Author Manuscript Author Manuscript Author Manuscript

9. Edwards AO, Ritter R III Abel KJ Manning A, Panhuysen C, Farrer LA. Complement factor H polymorphism and age-related macular degeneration. Science. 2005;308:421–424. [PubMed: 15761121]
10. Gold B, Merriam JE, Zernant J, et al. Variation in factor B (BF) and complement component 2 (C2) genes is associated with age-related macular degeneration. Nat Genet. 2006;38:458–462. [PubMed: 16518403]
11. Hageman GS, Anderson DH, Johnson LV, et al. A common haplotype in the complement regulatory gene factor H (HF1/CFH) predisposes individuals to age-related macular degeneration. Proc Natl Acad Sci USA. 2005;102:7227–7232. [PubMed: 15870199]
12. Haines JL, Hauser MA, Schmidt S, et al. Complement factor Hvariant increases the risk of age-related macular degeneration. Science. 2005;308:419–421. [PubMed: 15761120]
13. Jakobsdottir J, Conley YP, Weeks DE, Mah TS, Ferrell RE, Gorin MB. Susceptibility genes for age-related maculopathy on chromosome 10q26. Am J Hum Genet. 2005;77:389–407. [PubMed: 16080115]
14. Klein RJ, Zeiss C, Chew EY, et al. Complement factor H polymorphism in age-related macular degeneration. Science. 2005;308: 385–389. [PubMed: 15761122]
15. Rivera A, Fisher SA, Fritsche LG, et al. Hypothetical LOC387715 is a second major susceptibility gene for age-related macular degeneration, contributing independently of complement factor H to disease risk. Hum Mol Genet. 2005;14:3227–3236. [PubMed: 16174643]
16. Yang Z, Camp NJ, Sun H, et al. A variant of the HTRA1 gene increases susceptibility to age-related macular degeneration. Science. 2006;314:992–993. [PubMed: 17053109]
17. Beatty S, Koh H, Phil M, Henson D, Boulton M. The role of oxidative stress in the pathogenesis of age-related macular degeneration. Surv Ophthalmol. 2000;45:115–134. [PubMed: 11033038]
18. Gomes A, Fernandes E, Lima JL. Fluorescence probes used for detection of reactive oxygen species. J Biochem Biophys Methods. 2005;65:45–80. [PubMed: 16297980]
19. Li Y, Huang TT, Carlson EJ, et al. Dilated cardiomyopathy and neonatal lethality in mutant mice lacking manganese superoxide dismutase. Nat Genet. 1995;11:376–381. [PubMed: 7493016]
20. Sandbach JM, Coscun PE, Grossniklaus HE, Kokoszka JE, Newman NJ, Wallace DC. Ocular pathology in mitochondrial superoxide dismutase (Sod2)-deficient mice. Invest Ophthalmol Vis Sci. 2001; 42:2173–2178. [PubMed: 11527927]
21. Gorbatyuk MS, Pang JJ, Thomas J Jr., Hauswirth WW, Lewin AS. Knockdown of wild-type mouse rhodopsin using an AAV vectored ribozyme as part of an RNA replacement approach. Mol Vis. 11:648–656 2005. [PubMed: 16145542]
22. Liu J, Timmers AM, Lewin AS, Hauswirth WW. Ribozyme knock-down of the gamma-subunit of rod cGMP phosphodiesterase alters the ERG and retinal morphology in wild-type mice. Invest Ophthalmol Vis Sci. 2005;46:3836–3844. [PubMed: 16186371]
23. Qi X, Lewin AS, Hauswirth WW, Guy J. Optic neuropathy induced by reductions in mitochondrial superoxide dismutase. Invest Ophthalmol Vis Sci. 2003;44:1088–1096. [PubMed: 12601034]
24. Crabb JW, Miyagi M, Gu X, et al. Drusen proteome analysis: an approach to the etiology of age-related macular degeneration. Proc Natl Acad Sci USA. 2002;99:14682–14687. [PubMed: 12391305]
25. Sparrow JR, Fishkin N, Zhou J, et al. A2E, a byproduct of the visualcycle. Vision Res. 2003;43:2983–2990. [PubMed: 14611934]
26. Zolotukhin S, Potter M, Zolotukhin I, et al. Production and purification of serotype 1, 2, and 5 recombinant adeno-associated viral vectors. Methods. 2002;28:158–167. [PubMed: 12413414]
27. Timmers AM, Zhang H, Squitieri A, Gonzalez-Pola C. Subretinal injections in rodent eyes: effects on electrophysiology and histology of rat retina. Mol Vis. 2001;7:131–137. [PubMed: 11435999]
28. Bligh EG, Dyer WJ. A rapid method of total lipid extraction and purification. Can J Biochem Physiol. 1959;37:911–917. [PubMed: 13671378]
29. Gu X, Meer SG, Miyagi M, et al. Carboxyethylpyrrole protein adducts and autoantibodies, biomarkers for age-related macular degeneration. J Biol Chem. 2003;278:42027–42035. [PubMed: 12923198]

Author Manuscript Author Manuscript Author Manuscript Author Manuscript

30. Kim SR, Fishkin N, Kong J, Nakanishi K, Allikmets R, Sparrow JR. Rpe65 Leu450Met variant is associated with reduced levels of the retinal pigment epithelium lipofuscin fluorophores A2E and isoA2E. Proc Natl Acad Sci USA. 2004;101:11668–11672. [PubMed: 15277666]
31. Anuradha CD, Kanno S, Hirano S. Oxidative damage to mitochondria is a preliminary step to caspase-3 activation in fluoride-induced apoptosis in HL-60 cells. Free Radic Biol Med. 2001;31:367–373. [PubMed: 11461774]
32. Wyllie AH. Glucocorticoid-induced thymocyte apoptosis is associated with endogenous endonuclease activation. Nature. 1980;284: 555–556. [PubMed: 6245367]
33. Auricchio A, Kobinger G, Anand V, et al. Exchange of surface proteins impacts on viral vector cellular specificity and transduction characteristics: the retina as a model. Hum Mol Genet. 2001; 10:3075–3081. [PubMed: 11751689]
34. Shen J, Yang X, Dong A, et al. Oxidative damage is a potential cause of cone cell death in retinitis pigmentosa. J Cell Physiol. 2005;203:457–464. [PubMed: 15744744]
35. Deeb RS, Hao G, Gross SS, et al. Heme catalyzes tyrosine 385 nitration and inactivation of prostaglandin H2 synthase-1 by peroxynitrite. J Lipid Res. 2006;47:898–911. [PubMed: 16470026]
36. Ebrahem Q, Renganathan K, Sears J, et al. Carboxyethylpyrrole oxidative protein modifications stimulate neovascularization: implications for age-related macular degeneration. Proc Natl Acad Sci USA. 2006;103:13480–13484. [PubMed: 16938854]
37. Murray J, Taylor SW, Zhang B, Ghosh SS, Capaldi RA. Oxidative damage to mitochondrial complex I due to peroxynitrite: identification of reactive tyrosines by mass spectrometry. J Biol Chem. 2003;278:37223–37230. [PubMed: 12857734]
38. Esterbauer H, Schaur RJ, Zollner H. Chemistry and biochemistry of 4-hydroxynonenal, malonaldehyde and related aldehydes. Free Radic Biol Med. 1991;11:81–128. [PubMed: 1937131]
39. Uchida K 4-Hydroxy-2-nonenal: a product and mediator of oxidative stress. Prog Lipid Res. 2003;42:318–343. [PubMed: 12689622]
40. Dunaief JL, Dentchev T, Ying GS, Milam AH. The role of apoptosisin age-related macular degeneration. Arch Ophthalmol. 2002;120: 1435–1442. [PubMed: 12427055]
41. Doonan F, Donovan M, Cotter TG. Caspase-independent photoreceptor apoptosis in mouse models of retinal degeneration. J Neurosci. 2003;23:5723–5731. [PubMed: 12843276]
42. Doonan F, Donovan M, Cotter TG. Activation of multiple pathways during photoreceptor apoptosis in the rd mouse. Invest Ophthalmol Vis Sci. 2005;46:3530–3538. [PubMed: 16186330]
43. Grossniklaus HE, Green WR. Histopathologic and ultrastructural findings of surgically excised choroidal neovascularization: Submacular Surgery Trials Research Group. Arch Ophthalmol. 1998; 116:745–749. [PubMed: 9639442]
44. Kimura K, Isashiki Y, Sonoda S, Kakiuchi-Matsumoto T, Ohba N. Genetic association of manganese superoxide dismutase with exudative age-related macular degeneration. Am J Ophthalmol. 2000;130:769–773. [PubMed: 11124296]
45. Kasahara E, Lin LR, Ho YS, Reddy VN. SOD2 protects against oxidation-induced apoptosis in mouse retinal pigment epithelium: implications for age-related macular degeneration. Invest Ophthalmol Vis Sci. 2005;46:3426–3434. [PubMed: 16123448]
46. Gosbell AD, Stefanovic N, Scurr LL, et al. Retinal light damage: structural and functional effects of the antioxidant glutathione peroxidase-1. Invest Ophthalmol Vis Sci. 2006;47:2613–2622. [PubMed: 16723478]
47. Imamura Y, Noda S, Hashizume K, et al. Drusen, choroidal neovascularization, and retinal pigment epithelium dysfunction in SOD1-deficient mice: a model of age-related macular degeneration. Proc Natl Acad Sci USA. 2006;103:11282–11287. [PubMed: 16844785]
48. Age-Related Eye Disease Study Group. A randomized, placebo-controlled, clinical trial of high-dose supplementation with vitamins C and E, beta carotene, and zinc for age-related macular degeneration and vision loss: AREDS report no. 8. Arch Ophthalmol. 2001;119:1417–1436. [PubMed: 11594942]
49. Delcourt C, Diaz JL, Ponton-Sanchez A, Papoz L. Smoking and age-related macular degeneration: the POLA Study. Pathologies Oculaires Liees a l'Age. Arch Ophthalmol. 1998;116:1031–1035. [PubMed: 9715683]

Author Manuscript Author Manuscript Author Manuscript Author Manuscript

50. Klein R, Klein BE, Linton KL, DeMets DL. The Beaver Dam Eye Study: the relation of age-related maculopathy to smoking. Am J Epidemiol. 1993;137:190–200. [PubMed: 8452123]
51. Smith W, Mitchell P, Leeder SR. Smoking and age-related maculopathy. The Blue Mountains Eye Study. Arch Ophthalmol. 1996; 114:1518–1523. [PubMed: 8953988]
52. Vingerling JR, Hofman A, Grobbee DE, de Jong P. Age-related macular degeneration and smoking. The Rotterdam Study. Arch Ophthalmol. 1996;114:1193–1196. [PubMed: 8859077]
53. Espinosa-Heidmann DG, Suner IJ, Catanuto P, et al. Cigarette smoke-related oxidants and the development of sub-RPE deposits in an experimental animal model of dry AMD. Invest Ophthalmol Vis. Sci. 2006;47:729–737. [PubMed: 16431974]
54. Chen C, Wu L, Wu D, et al. The local cone and rod system function in early age-related macular degeneration. Doc Ophthalmol. 2004; 109:1–8. [PubMed: 15675195]
55. Feigl B, Brown B, Lovie-Kitchin J, Swann P. The rod-mediated multifocal electroretinogram in aging and in early age-related maculopathy. Curr Eye Res. 2006;31:635–644. [PubMed: 16877272]
56. Dandekar SS, Jenkins SA, Peto T, et al. Autofluorescence imaging of choroidal neovascularization due to age-related macular degeneration. Arch Ophthalmol. 2005;123:1507–1513. [PubMed: 16286612]
57. Sparrow JR, Zhou J, Ben Shabat S, Vollmer H, Itagaki Y, Nakanishi K. Involvement of oxidative mechanisms in blue-light-induced damage to A2E-laden RPE Invest Ophthalmol Vis Sci. 2002;43: 1222–1227. [PubMed: 11923269]
58. Sparrow JR, Cai B. Blue light-induced apoptosis of A2E-containingRPE: involvement of caspase-3 and protection by Bcl-2. Invest Ophthalmol Vis Sci. 2001;42:1356–1362. [PubMed: 11328751]
59. Bailey TA, Kanuga N, Romero IA, Greenwood J, Luthert PJ, Cheetham ME. Oxidative stress affects the junctional integrity of retinal pigment epithelial cells Invest Ophthalmol Vis Sci. 2004; 45:675–684. [PubMed: 14744914]
60. Cai J, Wu M, Nelson KC, Sternberg P Jr, Jones DP. Oxidant-induced apoptosis in cultured human retinal pigment epithelial cells. Invest Ophthalmol Vis Sci. 1999;40:959–966. [PubMed: 10102293]
61. Zeitz O, Schlichting L, Richard G, Strauss O. Lack of antioxidative properties of vitamin C and pyruvate in cultured retinal pigment epithelial cells. Graefes Arch Clin Exp Ophthalmol. Published online 7 26, 2006.
62. Cideciyan AV, Hood DC, Huang Y, et al. Disease sequence from mutant rhodopsin allele to rod and cone photoreceptor degeneration in man. Proc Natl Acad Sci USA. 1998;95:7103–7108. [PubMed: 9618546]
63. Cruickshanks KJ, Klein R, Klein BE. Sunlight and age-related macular degeneration. The Beaver Dam Eye Study. Arch Ophthalmol. 1993;111:514–518. [PubMed: 8470986]
64. Vaughan DK, Coulibaly SF, Darrow RM, Organisciak DT. A morphometric study of light-induced damage in transgenic rat models of retinitis pigmentosa. Invest Ophthalmol Vis Sci. 2003;44:848–855. [PubMed: 12556421]
65. Wang F, Rendahl KG, Manning WC, Quiroz D, Coyne M, Miller SS.AAV-mediated expression of vascular endothelial growth factor induces choroidal neovascularization in rat. Invest Ophthalmol Vis Sci. 2003;44:781–790. [PubMed: 12556414]
66. Ambati J, Anand A, Fernandez S, et al. An animal model of age-related macular degeneration in senescent Ccl-2- or Ccr-2-deficient mice. Nat Med. 2003;9:1390–1397. [PubMed: 14566334]
67. Malek G, Johnson LV, Mace BE, et al. Apolipoprotein E allele-dependent pathogenesis: a model for age-related retinal degeneration. Proc Natl Acad Sci USA. 2005;102:11900–11905. [PubMed: 16079201]

Author Manuscript Author Manuscript Author Manuscript Author Manuscript

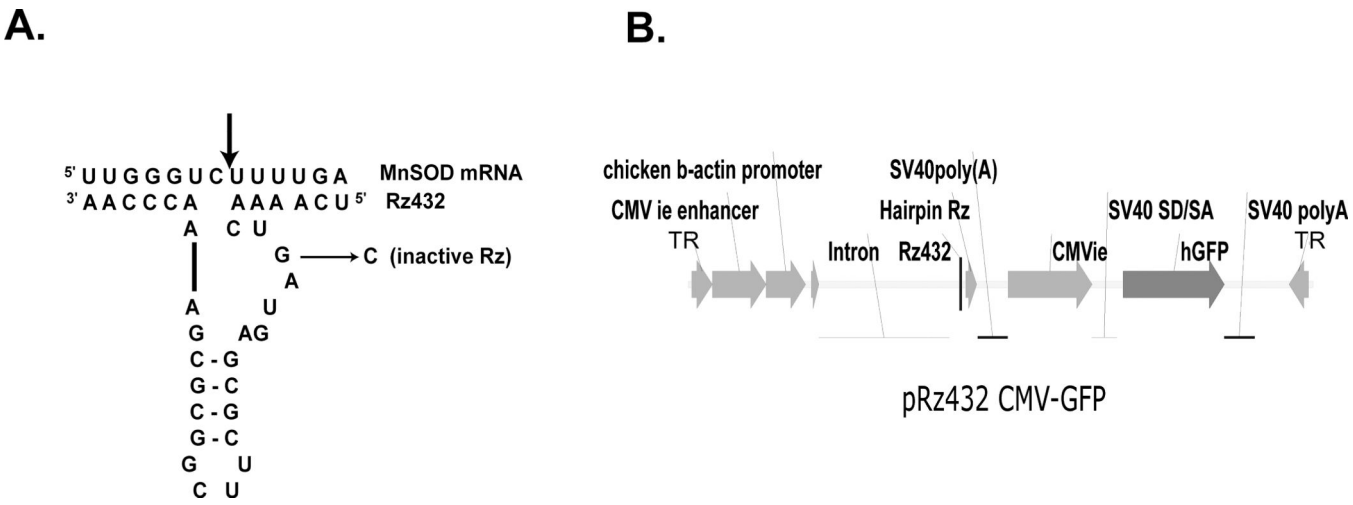

Figure 1.

Secondary structure of hammerhead ribozyme targeting the MnSOD and AAV packaging construct. (**A**) Sequence of MnSOD Rz432 and its MnSOD mRNA targeting sequence with cleavage site (*thick arrow*). Nucleotide position change to produce inactive MnSOD Rz432 (*thin arrow*). (**B**) The recombinant AAV cassette used to produce CBA-SOD2Rz432/CMV-GFP viral vector. TR, inverted terminal repeats; CMV, cytomegalovirus; CBA, chicken β-actin; SD/SA, splice donor/acceptor site; hGFP, humanized green fluorescent protein.

Author Manuscript Author Manuscript Author Manuscript Author Manuscript

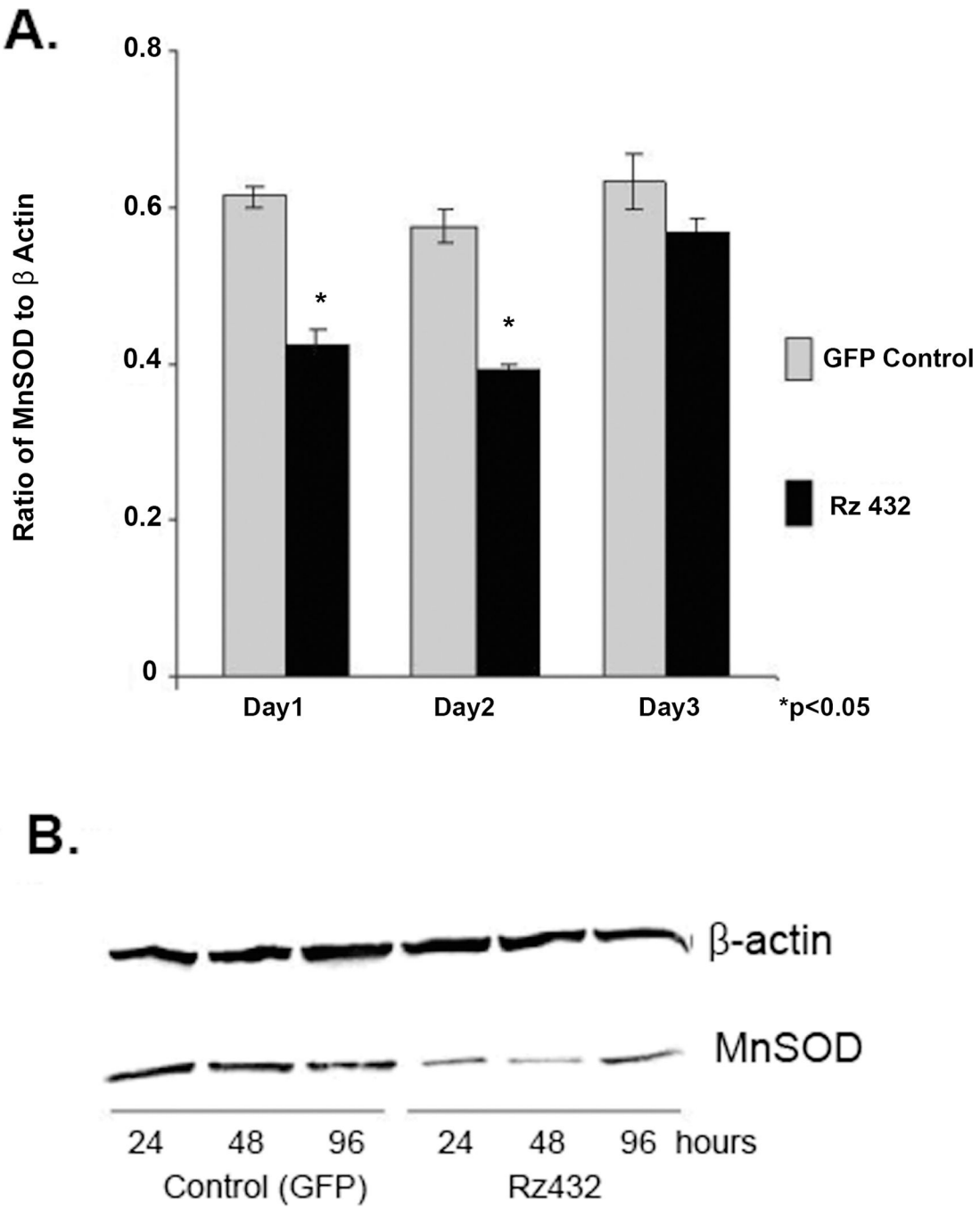

Figure 2.

Effects of Rz432 on MnSOD expression in RPE-J cells. (**A**) Quantification of MnSOD transcript levels measured in triplicate with reverse transcription PCR. β-Actin amplified in the same reactions was used as an internal control. PCR products were quantitated by SYBR green staining. A significant decrease in MnSOD transcripts was observed by 24 hours after treatment with Rz432 ($P < 0.05$). (**B**) Western blot for MnSOD protein levels from Rz432 or GFP-treated cells. MnSOD mRNA and protein levels returned to normal after 4 days,

because of the transient transfection. This experiment was performed twice, with essentially identical results.

Author Manuscript Author Manuscript Author Manuscript Author Manuscript

Author Manuscript Author Manuscript Author Manuscript Author Manuscript

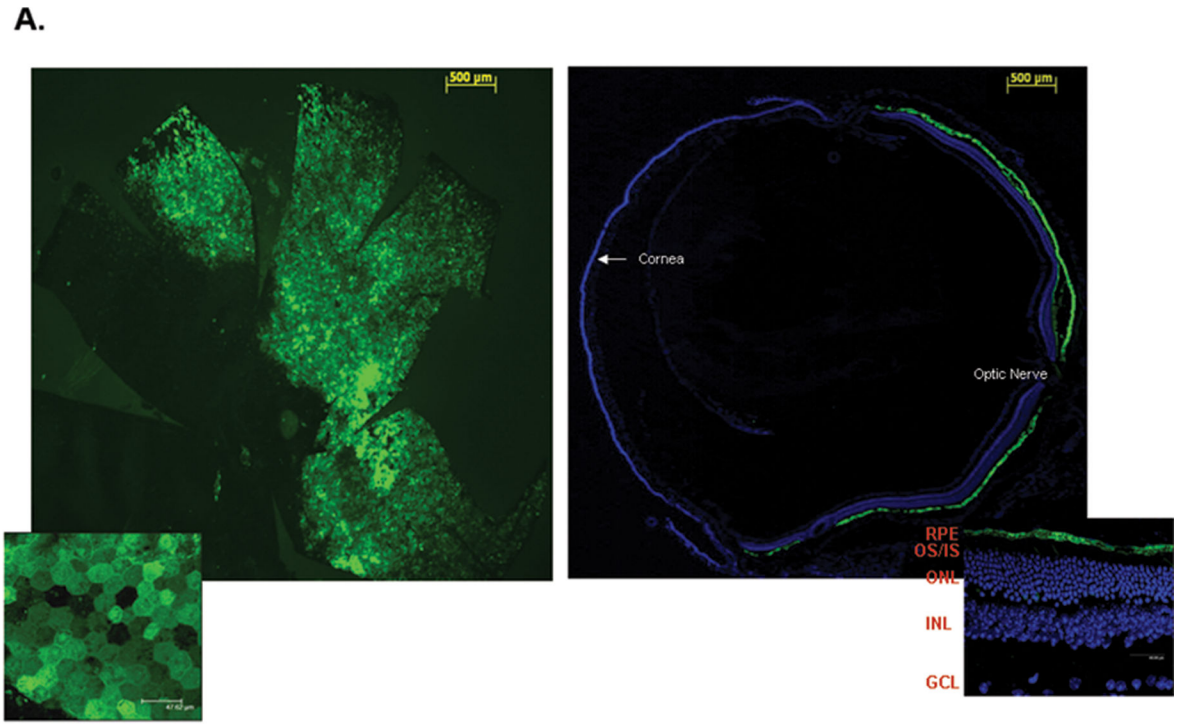

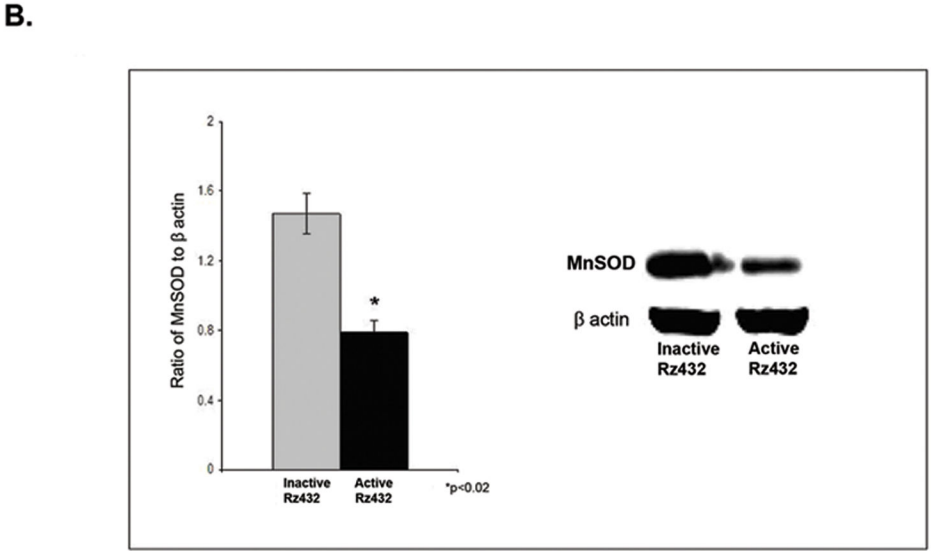

Figure 3.

Expression of Rz432 in RPE reduced MnSOD protein in the retina. (**A**) Localization of Rz432-GFP expression at 6 weeks after injection (*green*). *Left*: a whole-mounted retina viewed from the anterior surface. *Inset*: higher magnification showing GFP transduction of hexagonal RPE cells. *Right*: a transverse section through the retina counterstained with DAPI to show cell nuclei (*blue*). A single injection of the vector transduced almost the entire span of the RPE. *Inset*: higher magnification illustrates that cells of the RPE and not photoreceptors were transduced. (**B**) Rz432 expression reduces MnSOD protein levels in the

Author Manuscript Author Manuscript Author Manuscript Author Manuscript

RPE/choroid. Groups of mice were analyzed by Western blot for MnSOD levels at 6 weeks after injection (*left*). β-Actin was used as a loading control. Graph shows the ratio of MnSOD to β-actin signal ($n = 6$). Representative immunoblot of MnSOD protein from RPE/choroid of Rz432 and inactive Rz-treated eyes (*right*).

Author Manuscript Author Manuscript Author Manuscript Author Manuscript

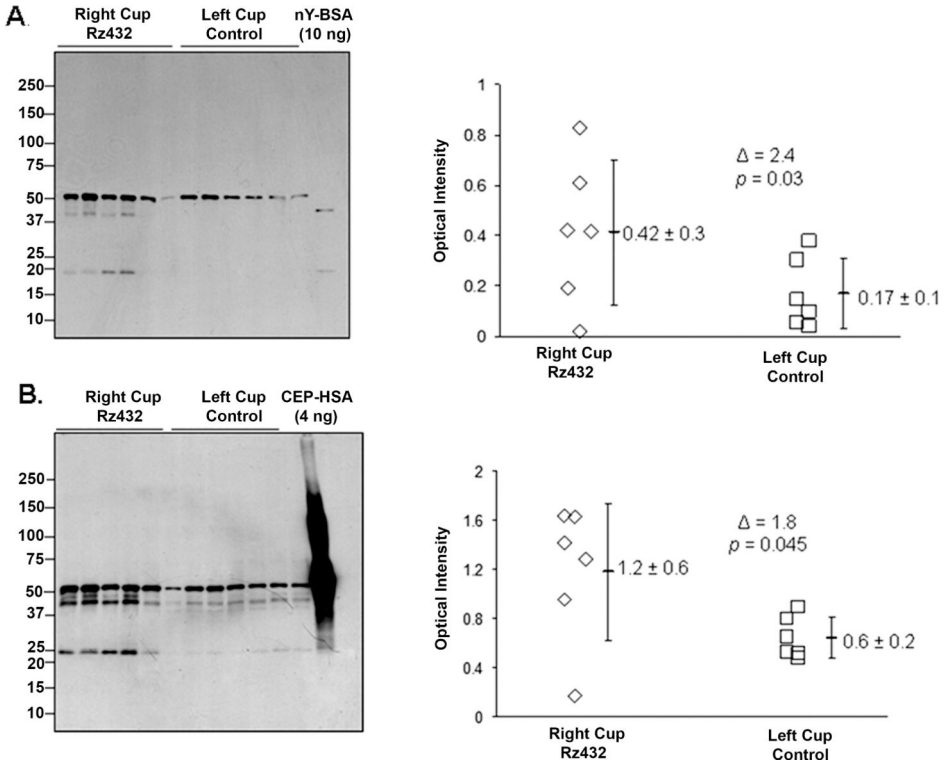

Figure 4.

Suppression of MnSOD2 led to accumulation of markers of oxidative stress. Western blot analysis of nitrotyrosine (**A**) and carboxyethylpyrrole (**B**) were performed with protein extracts of posterior eye cups. Rz432-treated eyes show significantly increased staining of bands immunoreactive for nitrotyrosine and carboxyethylpyrrole (immunoblots). The nitrotyrosine and carboxyethylpyrrole bands were quantitated by scanning and measuring optical densities (scatterplots). (◇) Rz432 treated; (□) control. ($P < 0.03$ for nitrotyrosine and $P < 0.045$ for carboxyethylpyrrole; $n = 6$).

Author Manuscript Author Manuscript Author Manuscript Author Manuscript

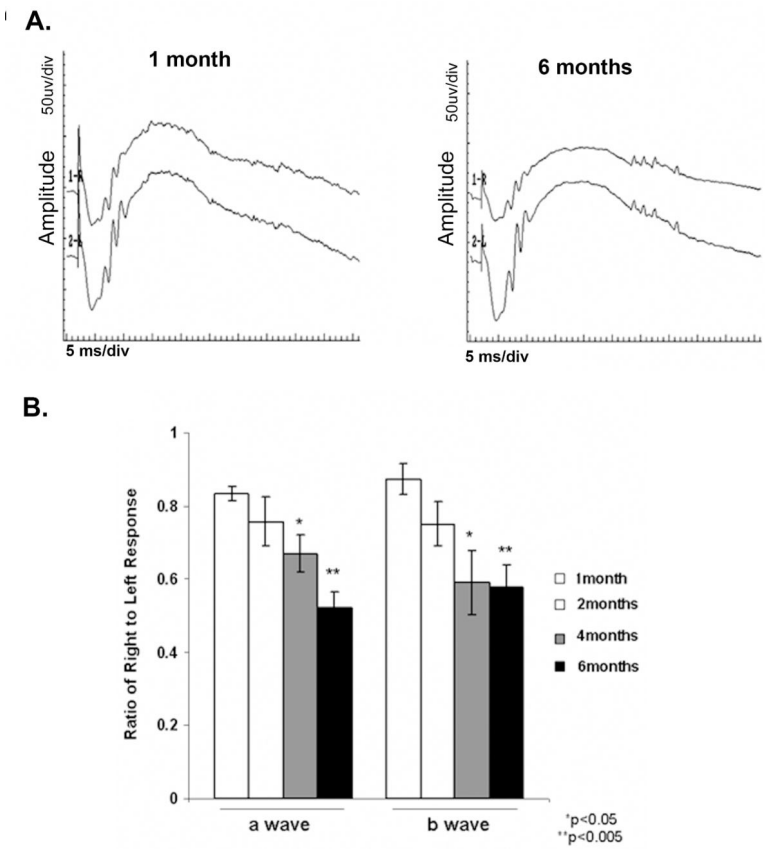

Figure 5.

Treatment of wild-type mice with Rz432 led to reduced light response. (**A**) Scotopic full-field ERGs were measured at 1, 2, 4, and 6 months after injection in groups of adult wild-type C57BL/6 mice injected with AAV-Rz432 or AAV-GFP control vector. Representative ERG waveforms from the 1- and 6-month time points are shown. R (right eye), AAV-Rz432; L (left eye), AAV-GFP control vector. (**B**) Mice treated with Rz432 showed progressive loss of ERG response that was significant by 4 months after injection. The graph represents the ratio of the maximum a- and b-wave amplitudes of Rz432 to GFP control. *$P < 0.05$; **$P < 0.005$. Error bars, SEM.

Author Manuscript Author Manuscript Author Manuscript Author Manuscript

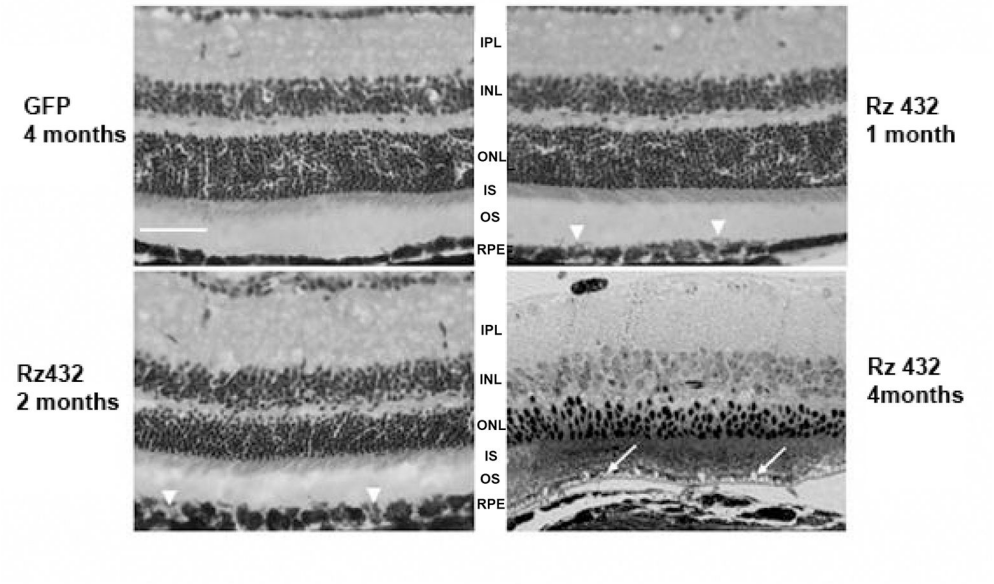

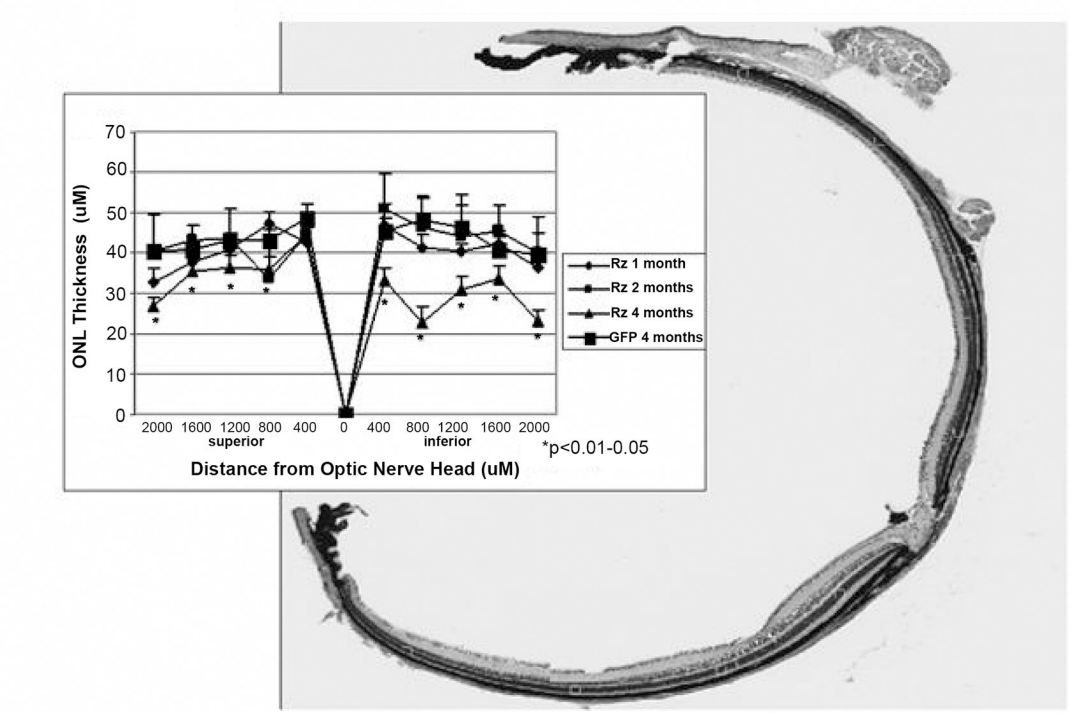

Author Manuscript Author Manuscript Author Manuscript Author Manuscript

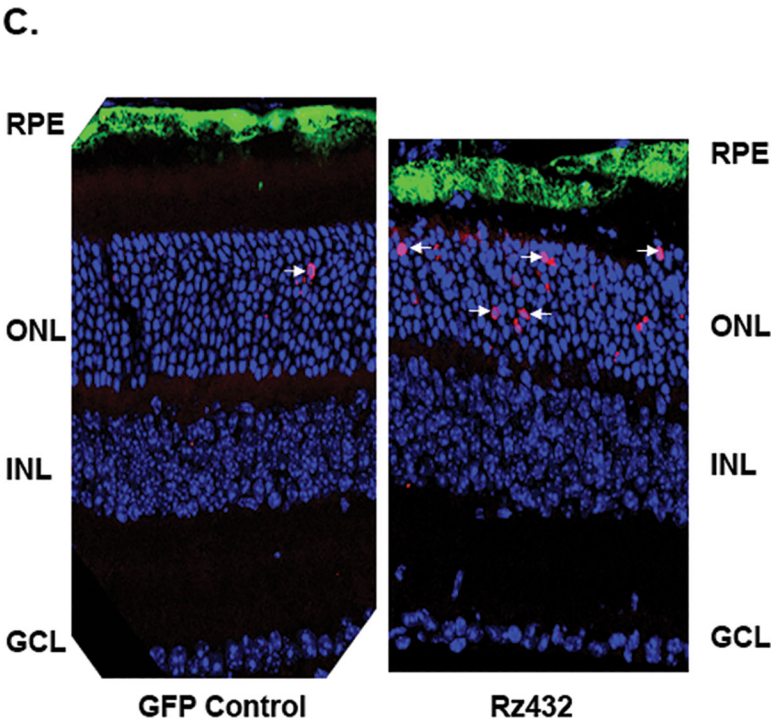

Author Manuscript Author Manuscript Author Manuscript Author Manuscript

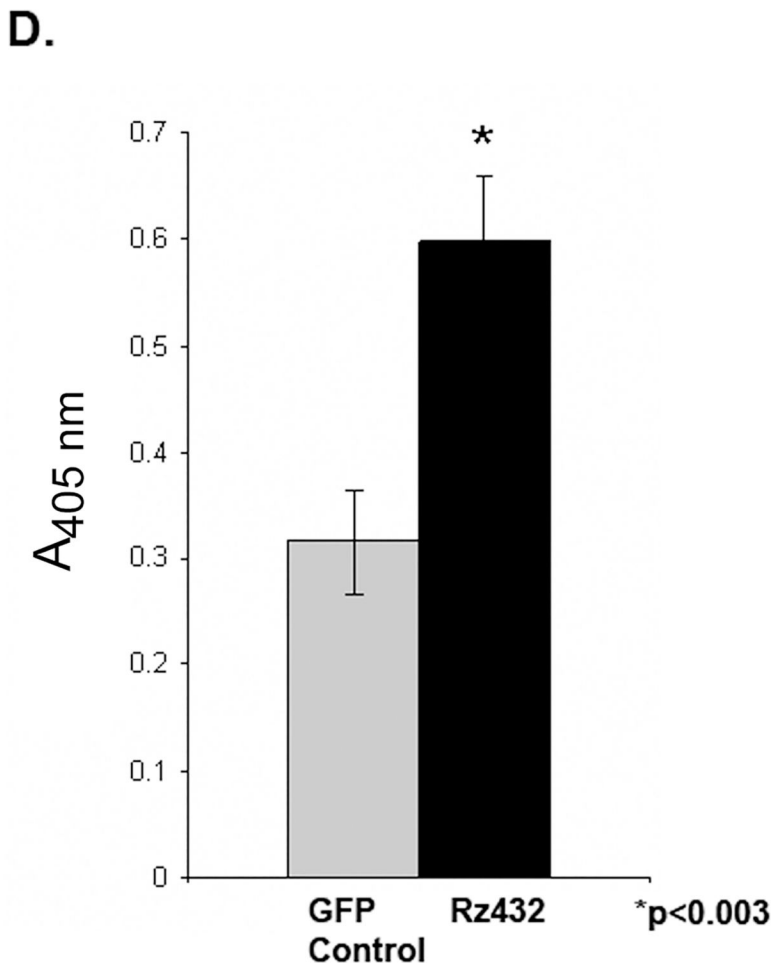

Figure 6.

Rz432 caused histologic damage to the outer retinas of mice. (**A**) Light micrographs of retinas of C57BL/6 mice at 1, 2, and 4 months after treatment with Rz432 or 4 months after treatment with GFP control vector. Rz432-treated retinas showed pigmentary changes (*arrow-heads*) and degeneration of the RPE (*arrow*) as well as progressive thinning of the photoreceptor nuclear layer. RPE, retinal pigmented epithelium; OS, photoreceptor outer segments; IS, photoreceptor inner segments; ONL, outer nuclear layer; INL, inner nuclear layer; IPL, inner plexiform layer. Scale bar, 50 μm. (**B**) Quantification of the thickness of the ONL. With the optic nerve head serving as a landmark, measurements were taken at 200-μm increments from the optic nerve on both the superior and inferior portions of the retina (n = 3 for each time point). Error bars, SEM *P < 0.05–P < 0.01. (**C**) Progressive loss of photoreceptor cells was due to apoptotic cell death. TUNEL staining was used to detect apoptotic nuclei in the retina at 6 weeks after Rz432 treatment (*left*). *Green*: Rz432-GFP expression; *red*: TUNEL-positive nuclei; *blue*, DAPI stained nuclei. (**D**) Quantification of apoptotic cell death by nucleosome release assay at 6 weeks after injection (*right*). *P < 0.003 (n = 6).

Author Manuscript Author Manuscript Author Manuscript Author Manuscript

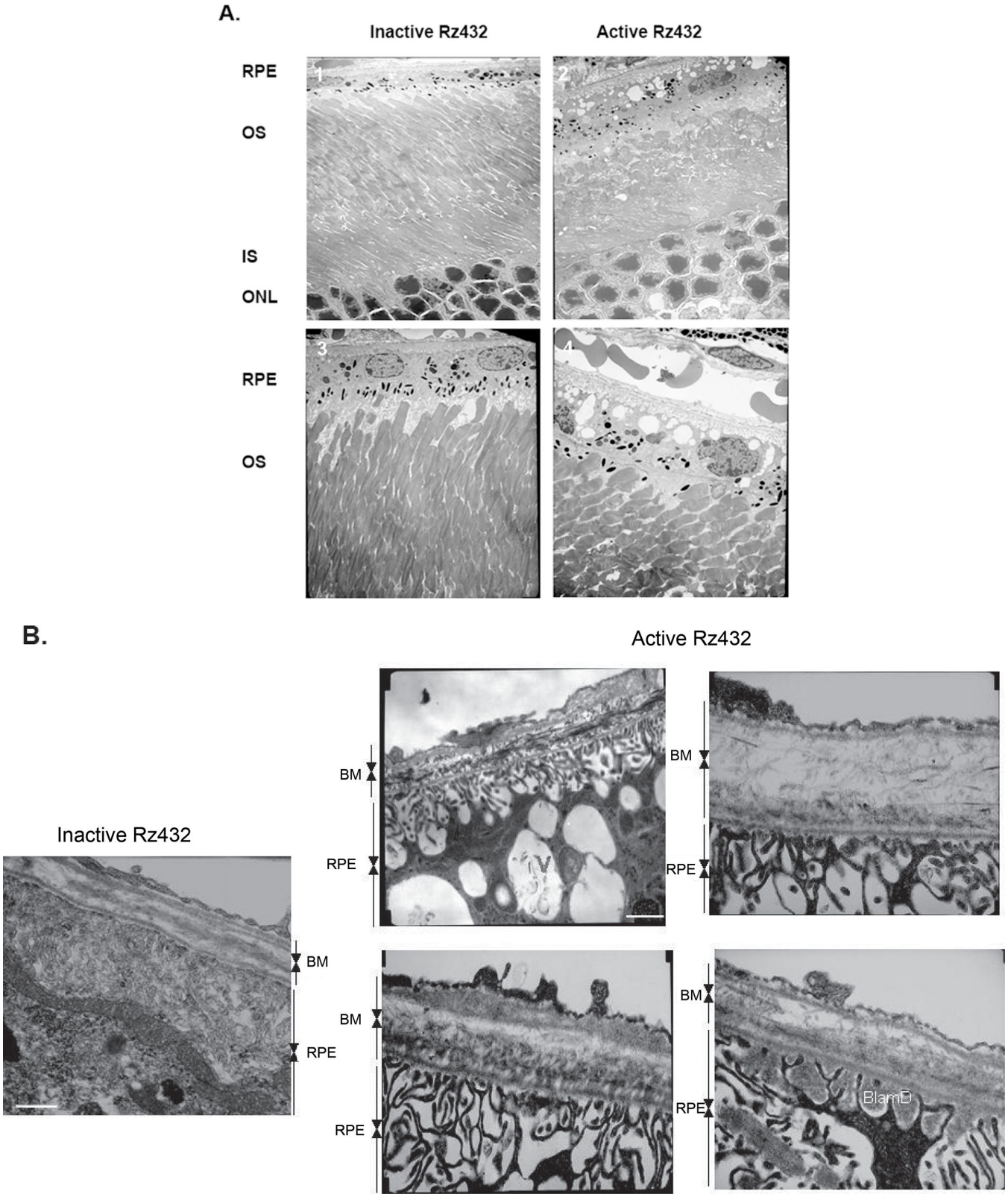

Figure 7.

Author Manuscript Author Manuscript Author Manuscript Author Manuscript

Ultrastructural changes in the outer retina at 4 months after AAV-Rz432 treatment. (**A**) Active Rz432-treated retinas (**A2**, **A4**) compared with control inactive Rz432-injected retinas (**A1**, **A3**), the RPE appeared distended with increased vacuolization and irregularly shaped nuclei. The outer and inner segments of the photoreceptors were shortened and disorganized. (**B**) Electron micrographs of Rz432 treated retinas showing unusual deposits between the plasma and basement membrane of the RPE as well as disorganization and increased thickening in the layers of Bruch's membrane. BlamD, basal laminar deposits. Scale bar (**A1, A2**) 10 μm; (**A3**, **A4**) 5 μm; (**B**) 0.5 μm.

Author Manuscript Author Manuscript Author Manuscript Author Manuscript

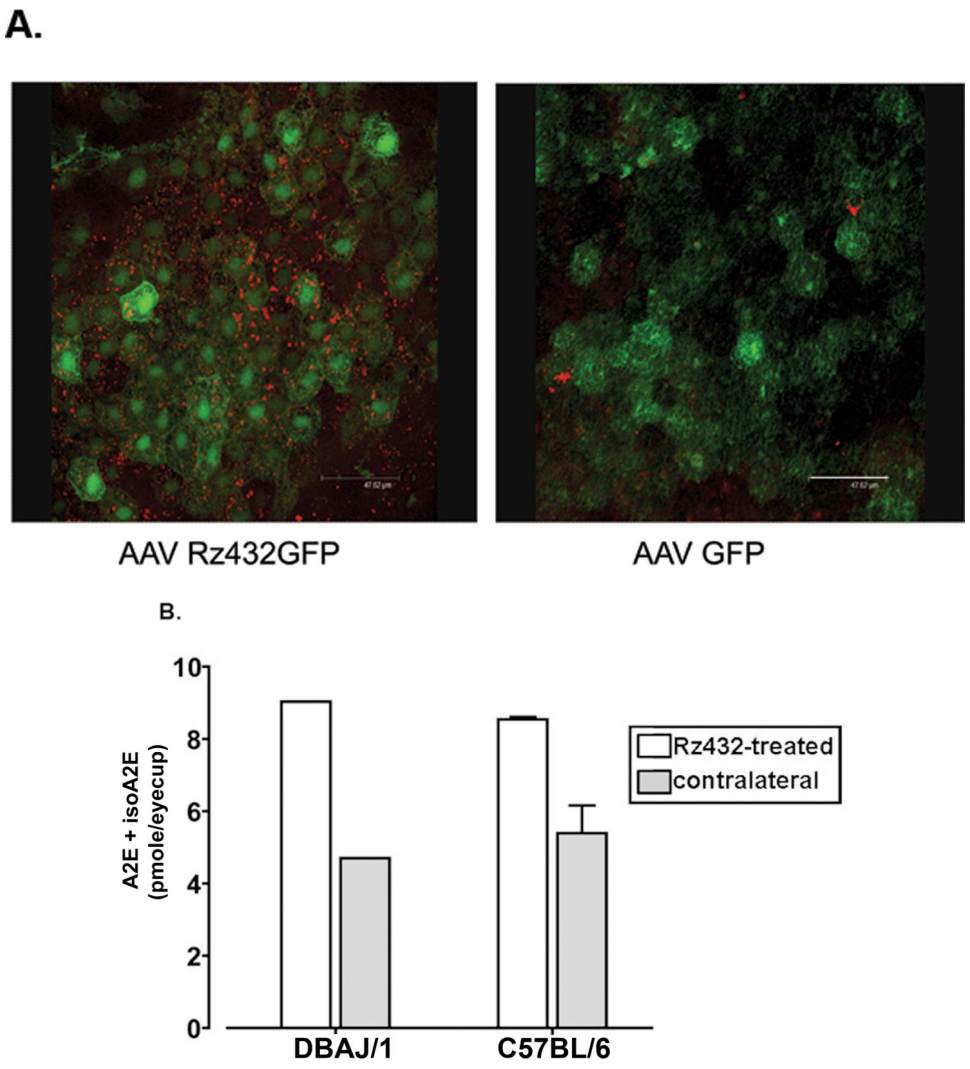

Figure 8.

Increased autofluorescence in oxidatively stressed retinas. (**A**) At 4.5 months after injection, flatmounts of the RPE/choroid/sclera were prepared from eyes fixed with paraformaldehyde and examined by fluorescence microscopy (excitation, 405 nm; emission, 590–650 nm) to detect autofluorescence in the presence of GFP fluorescence from the AAV vector. (**B**) Quantitation of A2E/iso-A2E in eyes of mice after ribozyme-mediated knockdown of SOD2. Mouse posterior eye cups were analyzed at age 4.5 months for DBAJ/1, which contains the Leu450 variant of RPE65, and at 5 to 6 months for C57BL/6J, which contains the Met450 variant of RPE65. Pigments were detected by HPLC with monitoring at 430 nm. A2E and iso-A2E levels were measured separately and summed. Results are based on single samples (4.5 months) or the mean (±SEM) of two samples (5–6 months). Each sample contained three to four eyes.

Author Manuscript Author Manuscript Author Manuscript Author Manuscript

Table 1.

Nitrated Proteins in SOD_{RZ}-Treated Mouse Posterior Eye Cup Identified by LC-MS/MS

Gel Band No.	Protein Name	Matched Peptide	Molecular Weight	Swiss-Prot Accession No.	Nitrotyrosine-Containing Peptide	Ion Score	E-Value Swiss-Prot (229K)	E-Value NCBI (4396K)
5	Transducin-like enhancer protein 3 (mouse)	1	83,160	Q08122	K.^{30}DEFQFLQAQ$^{@}$Y*HSLK^{43}.V	19	6e-08	4e-07
16	Elastase-1 precursor (rat)	1	28,822	P00773	K.^{52}WY*HTC$^{\#}$GGTLIR^{62}.Q	15	7e-06	5e-05
16	Fibroblast growth factor receptor 2 precursor (mouse)	1	91,984	P21803	R.^{650}DIN$^{@}$NIDY*YKK^{659}.T	18	2e-04	0.002
5	Early development regulatory protein 2 (p36) (mouse)	1	89,799	Q9QWH1	K.^{592}KY*AQ$^{@}$GFLPEK^{601}.P	33	0.001	0.009
12	Zinc finger protein 277 (human)	1	51,582	Q9NRM2	R.^{87}Y*ILY*WRKR^{94}.F	22	0.006	0.052
4	LIM/homeobox protein Lhx8 (mouse)	1	40,670	O35652	R.^{152}RY*GTRCSR^{159}.C	20	0.05	0.34
18	Growth factor independence 1 (mouse)	1	45,845	P70338	R.^{249}LLLGGGSY*K^{257}.C	16	0.076	0.52
18, 20	Apoptosis-inducing factor 2 (mouse)	1	40,609	Q8BUE4	K.^{247}IN$^{@}$SSAY*R^{253}.S	17	1.1	7.6

The sequence of each peptide was analyzed by BLAST against the Swiss-Prot and NCBI database and corresponding species. The sequence of each nitrated peptide matched exactly to the sequence of each protein, and that protein was the only one to be matched in Swiss-Prot database and corresponding species. The same protein was also exactly matched in NCBI database and corresponding species. E-Value, expectation value, the number of alignments with scores ≥ than the associated score expected to occur in a database search by chance. Y*, nitrated tyrosine; C$^{\#}$, carbamidomethylated Cys; N$^{@}$, deamidated Asn; Q$^{@}$, deamidated Gln.